JOURNAL OF MATERIALS SCIENCE 2 (1967) 221–232

# Deformation Mechanisms of Metals Hardened by a Dispersed, Incoherent, Second Phase

P. GUYOT*
*Metallurgy and Ceramics Division, Euratom, Ispra, Italy*
E. RUEDL
*Physical Chemistry Division, Euratom, Ispra, Italy*

*Received 15 February 1967*

Hardening of fcc metals by incoherent particles is analysed. The presence of the particles indirectly determines the rapid multiplication of dislocations in the matrix. The hardening is related to the dense tangles so formed. Recovery of these tangles occurs by cross-slip, climb, and probably by some other complex, thermally activated mechanisms.

## 1. Introduction

In recent years, the investigation of dispersion-strengthening of metals has shown that the hardening of the metal depends mainly on whether the discrete second-phase particles are sheared by the dislocations moving in the matrix. In this respect, the classification of hardening by a coherent or an incoherent† second phase can be adopted: the coherent phase is usually sheared, but not the incoherent phase.

Nevertheless, other factors, such as the size of the particles, also influence the shearing. When a dislocation, confined to slip in its glide plane, encounters particles, it may expand between them, leaving a residual loop around each particle, or it may shear them. The stress necessary in the first case, known as the Orowan stress [1], is $\tau_c \simeq \mu b/d$; where $\mu$ is the shear modulus of the matrix, $b$ the Burgers vector, and $d$ the inter-particle distance in the slip plane. For a given volume fraction of precipitate, $\tau_c$ decreases as the size of the particles increases. In the second case, the stress increases with the size of the particles. An upper limit for the radius of the particles to be sheared, $r_1$, can be obtained by equating the two stresses. The higher the inter-facial energy, the lower is the upper limit. Only those incoherent particles which are very small and which have a high interfacial energy, $\gamma$, can be sheared. For the aluminium-alumina system, taking $\gamma = 1000$ ergs/cm$^2$, an approximate calculation gives $r_1 = 15$ Å.

Therefore, a glide dislocation encountering such incoherent particles will generally expand between them or, alternatively, by-pass them by some more-complicated mechanisms, such as cross-slip or climb. The strain-hardening of these alloys, at least for sufficiently small deformations, is much higher than that of the pure matrix and is intimately related to the sub-structures of the alloy matrix. It will be shown that the hardening can, in effect, be explained in terms of the elastic interaction of the dislocations in the matrix. The second-phase particles play the indirect role of accelerating the increase in dislocation density with the strain, leading to steep strain-hardening. As we shall show below, this conclusion is in conflict with the Fisher-Hart-Pry model of dispersion-hardening (which is based on the notion that the particles accumulate dislocation loops which increase the effective size of the particles).

*Present address: Inorganic Materials Research Division, Lawrence Radiation Laboratory, and Department of Mineral Technology, College of Engineering, University of California, Berkeley, California.

†A "coherent" second phase is closely matched to the matrix in respect of orientation and lattice spacing, so that the interfacial energy is very low. An "incoherent" boundary, which does not meet these criteria, has a much larger inter-facial energy with respect to the matrix. Coherent particles can only be created by phase transformation.

On the other hand, direct dislocation-particle interactions are expected to control the hardening by coherent particles.

The purpose of this paper is to give a review of the results obtained on crystals containing uniformly distributed, incoherent particles. The true elastic limit will be briefly considered, and emphasis will be placed on the variation of the flow stress with temperature for macroscopic plastic deformation. In addition, an electron microscope study of Al-$Al_2O_3$ sintered-aluminium-powder (SAP) alloys is described, including examinations of particle/matrix interfaces and measurements of dislocation densities.

## 2. Elastic Limit

The particles intersecting the glide plane are anchoring points for the dislocation. As mentioned before, according to Orowan [1], the increase in the elastic limit relative to the pure matrix is $\simeq 2t/bd$, where $t$ is the line tension of the dislocation. The Orowan bowing applies, provided the dislocations are confined in their motion to the slip plane. Depending on whether the particles are elastically harder or softer than the matrix, the dislocation is repelled or attracted by the particles, and the anchoring is somewhat different in each case [2]. The Orowan criterion holds in both cases [3].

The Orowan relationship has been verified for single crystals containing uniformly distributed, small particles [4-6]. It must be pointed out that this law is expected to apply when the initial dislocation density is low enough for the particles to play the role of first obstacles.

Ashby [7], using an idea of Hirsch [8], proposed a by-pass of particles by double cross-slip, as schematically shown in fig. 1 for an edge dislocation. When the dislocation starts the

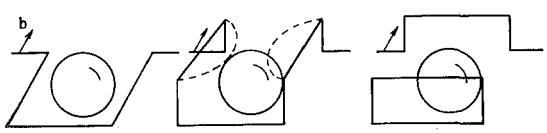


*Figure 1* Double cross-slip for an edge dislocation.

Orowan bowing, the resulting screw components cross-slip out of the slip plane under the action of the stress concentration near the particle. The cross-slipped segments attract each other, resulting, after annihilation, in a prismatic loop behind the particle and jogs in the dislocation line. Ansell [9] has shown that a restrictive geometrical condition (when $2r \leqslant d/10$, where $r$ is the radius of the particle) affects the by-pass by double cross-slip. Experimental evidence of this mechanism is limited to the prismatic loops observed by electron microscopy [7, 10, 11]. Because this cross-slip has to be thermally activated, the true elastic limit, if controlled by such a mechanism, has to vary more strongly with temperature than the elastic constants; this contradicts experimental evidence [10]. Nevertheless, it will be shown later that cross-slip occurs extensively after some plastic straining.

## 3. Temperature Variation of the Flow Stress

Here we summarise the results obtained by one of us (Guyot) on the polycrystalline Al-$Al_2O_3$ system (SAP) [12], and by Mitchell *et al* on the Al-$Al_2Cu$ system [14]. The flow mechanisms involved can probably be generalised for alloys with incoherent particles in a fcc matrix of high stacking-fault energy.

The composition and the structural parameters of the alloys, as determined by electron microscopy, are given in table I. While the $Al_2Cu$ ($\theta$ phase) particles are roughly spherical in shape, the alumina particles in SAP are platelets, with linear size between 200 and 2000 Å, and a thickness of about 200 Å. The $r$ given in table I for the mean, planar, particle radius is, in this latter case, the radius of a circle of the same area as that of the mean area of platelets intersected by a random plane, i.e. $r = (2Le/\pi)^{1/2}$, where $L$ is half of the mean linear size and $e$ is the thickness [12]. The temperature dependence of the

TABLE I Structure parameters of the alloys with dispersed, incoherent, second phase.

| Alloy type | Dispersed phase | $f$(%) | $r$($\mu$m) | $d$($\mu$m) | Grain size ($\mu$m) |
|---|---|---|---|---|---|
| SAP 4* | $Al_2O_3$ $\gamma$ | 2.75 | 0.025 | 0.20 | |
| SAP 7 | $Al_2O_3$ $\gamma$ | 4.85 | 0.029 | 0.18 | 2 to 5 |
| SAP 10 | $Al_2O_3$ $\gamma$ | 7.00 | 0.031 | 0.16 | |
| 4M | $Al_2Cu$ | 4.5 | 0.298 | 2.8 | 430 |
| 4C | $Al_2Cu$ | 4.5 | 1.08 | 11.4 | 410 |
| 5F | $Al_2Cu$ | 5.9 | 0.158 | 1.3 | 430 |

$f$ = volume fraction of dispersed phase
$r$ = mean, planar, particle radius
$d$ = mean, planar, inter-particle distance
*This number is the wt % of alumina.

deformation mechanisms controlling the flow stress is now discussed.

### 3.1. Flow Stress at Low Temperatures (ABC in fig. 2)

#### *3.1.1. Forest Process*

At low temperatures, and under small stresses for creep (or at low strain for tension at constant strain rate), the mobile dislocations cannot leave the glide plane. Their glide, in pure fcc metals, can be hindered both by long-range internal stresses and by short-range obstacles provided by the "trees" – dislocations piercing their glide plane. The deformation is then controlled by the thermally activated jog-formation, during cutting through those trees, and by the movement in long-range stress fields.

The tensile curves for both Al-$Al_2O_3$ and Al-$Al_2Cu$ systems, especially for small strains, present a strain-hardening rate which is much higher than that for polycrystalline aluminium [12-14] and largely dependent on the temperature.

The variations of the tensile flow stress, for a given strain rate, with temperature are shown schematically in fig. 2 (for three strains increasing from curves 1 to 3).

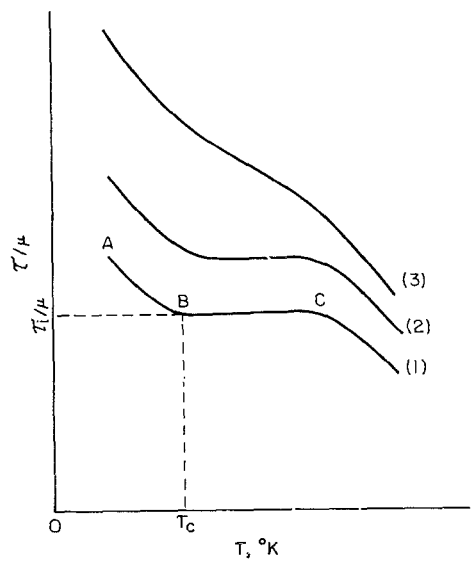


*Figure 2* Variations of the tensile flow stress, for different strains, as a function of temperature (the flow stress is corrected for the variations of the shear modulus $\mu$ with temperature).

The curves of type (1) or (2) are similar to those of pure metals, whose hardening is controlled by the forest process as mentioned before. The AB part in fig. 2 corresponds to the thermally activated jog-formation; whereas, in the BC part, the forest opposes the development of loops only by long-range internal stresses $\tau_i$. In fcc structures, the long-range stresses are principally due to the attractive trees giving junction reactions with the mobile dislocations [15].

An estimate of the energy of formation of a pair of jogs, $2U_{fc}$, can be deduced from the measurement of $T_c$,* according to Friedel's theory [2] as described in reference 12. The results so obtained are gathered in table II, for Al-$Al_2O_3$ and Al-$Al_2Cu$ alloys, and for two purities of aluminium. Applying the forest theory to the thermal decrease of $\tau$ at low temperatures, we thus obtain, for both alloys and aluminium, a common value of $2U_{fc}$; namely, $2U_{fc} = 0.37 \pm 0.05$ eV. A better estimate of $2U_{fc}$ is given by a direct measurement of the activation energy beyond $T_c$ [2]; the value so obtained for SAP 11.7† is $\simeq 0.35$ eV [12, 13], in good agreement with the former mean value, and of a reasonable order of magnitude for the energy of formation of a pair of jogs in aluminium. Thus, the activation energy is compatible with the forest process controlling the plastic deformation in these alloys, as in pure aluminium.

The measurement of the activation volume from strain-rate-change tensile tests allows the determination of the force-distance diagram, showing the elastic interaction between a repulsive tree (not giving a junction reaction) and a mobile dislocation. The results obtained by Mitchell *et al* for Al-$Al_2Cu$ and pure aluminium [14] and by Guyot for SAP and impure aluminium [12, 13]‡ are shown in fig. 3. The fact that these $F$-$x$ curves only differ a little is added evidence for the presence of the intersection mechanism in all these materials.

#### *3.1.2. Cross-Slip and Self-Diffusion*

For large strains (curve (3) in fig. 2), the shape of the curve of $\tau/\mu$ versus $T$ can no longer be explained solely with the mechanism of section 3.1.1. The absence of a plateau in this curve seems to be due to a strongly thermally activated mechanism. In fact, by measuring the activation

*$T_c$ is near to 173° K for SAP, for a strain rate of $2.7 \times 10^{-4}$ sec$^{-1}$ and at small strains ($< 2.10^{-3}$ %).
†i.e. SAP containing 11.7 wt % alumina.
‡The SAP matrix consists of impure aluminium (99.5 wt %).

TABLE II Energies of formation of a pair of jogs.

| Alloy | SAP 4.5 | SAP 11.7 | 4M | 4C | 5F | Al 99.5% | Al 99.9% |
|---|---|---|---|---|---|---|---|
| $2U_{fc}$ (eV) | 0.43 | 0.42 | 0.35 | 0.41 | 0.34 | 0.33 | 0.37 |

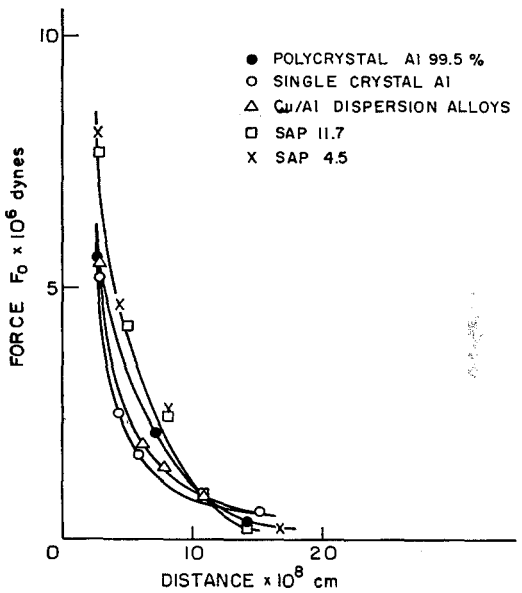


*Figure 3* Force-distance diagram.

energy, $\Delta H$, at constant strain rate as a function of temperature, we established that the change in shape of these curves is reflected by the curves of $\Delta H$ versus $T$ (fig. 4 for SAP 11.7) [12, 13]. At small strains, $\Delta H$ flattens out at

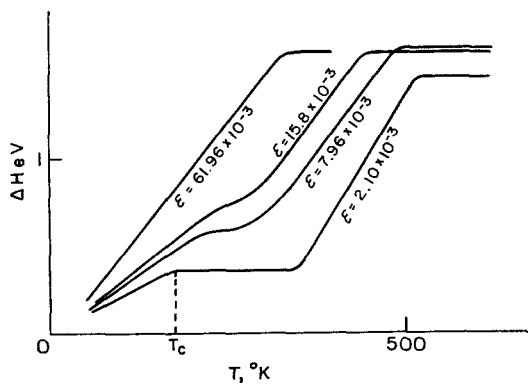


*Figure 4* Variations of the activation energy function of temperature, at constant strain rate ($\dot{\epsilon} \simeq 2.7 \times 10^{-4}$ sec$^{-1}$) and for different strains (SAP 11.7).

$\simeq 2U_{fc}$ for $T > T_c$, suggesting a forest process; but, for large strains, $\Delta H$ increases beyond $T_c$ and reaches a plateau at about 1.6 eV at high temperatures, clearly corresponding solely to the operation of a diffusion process. At intermediate temperatures, the variation of $\Delta H$ with $T$ probably corresponds to ill-defined cross-slip processes complicated by the effect of internal stresses. These phenomena should determine the relaxation of the internal stresses leading to the thermal decrease of $\tau$. The observation, by electron microscopy, of plastically deformed specimens shows a homogeneous distribution of dislocations when the deformation is low; while, after high deformations, the dislocations are tangled and have a cell structure [11, 16, 17]. Cells in SAP were observed only for high deformations and beyond the plateau $\tau$ ($T$).

As we saw previously, the cross-slip of screw dislocations should lead to a decrease in $\tau$ with increasing temperature and for high strains. Therefore, we can reasonably conclude that our observations agree with the idea that the cell formation is related to: (i) the cross-slip of screw dislocations; (ii) the decrease with temperature of the tensile stress after the plateau.

Thomas *et al* [18] suggested that the tangles and cells result from the multiplication of dislocations by operation of Frank-Read sources left by cross-slip of dislocations adjacent to particles. This could explain, for instance, why the cells observed in thoria-dispersed nickel (TD-Ni) appear to have corners located at the largest particles [18]. This mechanism of formation of cells is slightly different from the above – which is in fact the normal cell formation by cross-slip in pure metals – because it requires the further operation of sources resulting from cross-slip. Until more evidence is obtained, it cannot be considered as firmly established. As will be shown in the next section, the role of particles as multiplication centres is evident but not well defined.

### 3.1.3. Strain-Hardening

The measurement of $\tau_i$, the temperature-independent stress (part BC in fig. 2), leads directly to an estimate of the density of dislocations with $\rho = (\mu b/\beta\tau_i)^{-2}$ after Saada's relation [15], where $\beta \simeq 4$ in fcc structures.

On the other hand, when the forest process is controlling the deformation, the measurement of the activation volume $v^*$ gives another possibility of determination of $\rho$, namely $\rho \simeq (1.5\, b^2/v^*)^2$ [12].

Obviously, a direct determination of $\rho$ is feasible by transmission electron microscopy. The variations of $\rho$ with the strain, as determined from the activation volume and electron microscopy, were given in table I of reference 11, for SAP 4.5 deformed at room temperature. In the appendix, we describe how the dislocation density in SAP can be determined by electron microscopy.

For strains smaller than about 2%, it can be seen from reference 11 that the agreement between both methods is quite good. For high strains, when cross-slip becomes operative and introduces a cell structure, the density $\rho$, as determined from the activation volume, is on the whole close to the density as determined by electron microscopy in the cell walls (the density in the walls is between 2 and 4 times higher than the mean density). Thus, it seems that the activation volume is characteristic of a forest process for which the mobile dislocations have to cut through the cell walls.

From the preceding study, we can conclude that the hardening of these alloys has the same origin as in pure fcc metals. (Dispersions in bcc structures have not been studied seriously. The limited number of mechanical tests made by Sell *et al* [19] on dispersions of oxides, nitrides, and carbides in tungsten are not conclusive.)

Their larger strain-hardening is due to a more rapid increase of the dislocation density with plastic strain, as shown in fig. 5, after Mitchell *et al* [14]. Fig. 5 represents the variation of the reciprocal of the distance $L$ between trees as a function of strain. Similar results were obtained by Guyot for SAP [12, 13] and Thomas *et al* for TD-Ni [18]. For Al-$Al_2Cu$, $(d\tau/d\epsilon)_T$ decreases with increasing particle spacing, $d$, for a given volume fraction, $f$; for SAP, the work-hardening rate increases with increasing $f$ or decreasing $d$. Although no quantitative relation has been proposed, these results show that the particles are thus playing an indirect role of multiplying the dislocation density. However, the exact mode of multiplication is not well understood. The particles can be active by creating prismatic loops by a volume indentation effect, or when dislocations by-pass them by cross-slip. The particles can also act as barriers to moving dislocations nucleated at other sources, such as Frank-Read sources,

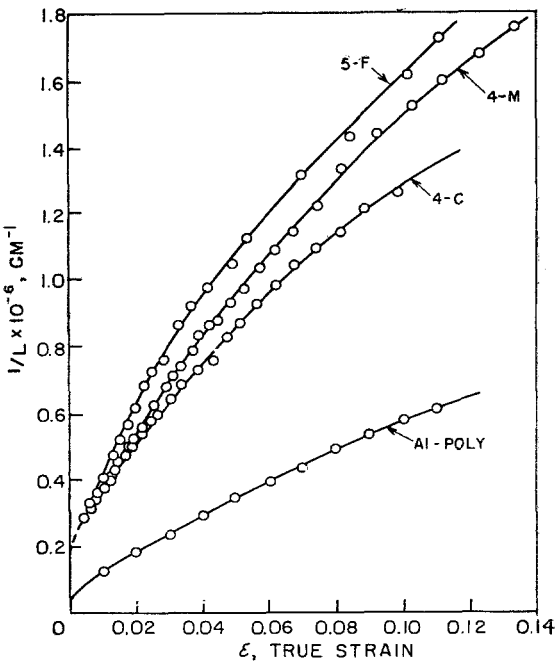


*Figure 5* Variation of $1/L$ with true strain.

grain boundaries, and twin boundaries in TD-Ni. This explains why, in both cases, the cell size seems to be governed by the particle spacing.

An interesting feature appears when studying the grain-size influence. As shown by Heimendahl and Thomas for TD-Ni [16], and by Guyot for SAP [12], the grain size has no influence either on the flow stress at 0.1 or 0.2% tensile strain or on the ultimate tensile stress. Transmission electron microscopy of tensile-strained recrystallised SAP shows that, for the same plastic strain, the dislocation density is about the same for as-extruded and recrystallised specimens. Thus, in recrystallised specimens, the dislocation density, initially low, increases very rapidly with deformation; and reaches, after a few tenths per cent of strain, a similar dislocation density, and therefore a similar flow stress, to that in the as-extruded material.*

Furthermore, the Fisher-Hart-Pry theory [20] of strain-hardening, based on the result of planar dislocation loops around the dispersed particles, is invalid. Since, as we saw, the role of the particles is to multiply the dislocations and enhance the cross-slip processes leading to a cell structure.

*For instance, the dislocation density measured in as-extruded SAP 4 (with an initial density of $\sim 5 \times 10^9/cm^2$) after 1% strain was $\sim 1.2 \times 10^{10}/cm^2$; whereas in recrystallised SAP 4 (with an initial density of the order of $10^7/cm^2$), after the same deformation, the dislocation density was $\sim 9 \times 10^9/cm^2$.

Ashby [17] proposed a somewhat more realistic model to account for the strain-hardening of these alloys, based on forest intersection. The strain-hardening was calculated assuming that the glide dislocations have to cut through the cell walls set up by the residual prismatic loops left by cross-slip on the particles (cf. section 2). Nevertheless, the assumed substructure is peculiar; even if such prismatic loops are observed, it is difficult to ascribe the work-hardening to their presence only. On the other hand, the formation of cell configurations takes place only at fairly high strains. At small strains, when the dislocations are uniformly distributed in the matrix, this theory is questionable. A pure forest process has to be considered. Unfortunately, in this case, the rate of increase of dislocation density with plastic strain is not clear.

### 3.2. Flow Stress at High Temperatures (above C in fig. 2)

The internal stresses related to the dislocation tangles are relieved at high temperatures by mechanisms common to pure metals (cross-slip and climb) and by some more-complicated mechanisms. This recovery is, however, strongly limited by the presence of the second phase, and the material will maintain high strength. The stability of the dislocation sub-structure is obviously a function of the dispersion stability; in this respect, oxide dispersions, which are very stable, will assure a good dislocation substructure at high temperatures, and therefore high strength.

These recovery processes can be analysed as a function of temperature from the spectrum of the activation energy, as determined by tensile tests for different grades of SAP and polycrystalline impure aluminium (99.5%) (fig. 6) [21].

#### *3.2.1. Cross-Slip and Self-Diffusion*

Between 100 and 350° C, for a strain of $2 \times 10^{-3}$, the movement of dislocations in the matrix is controlled by cross-slip and climb, as in pure aluminium (at same stress level, the cross-slip and self-diffusion energies in pure aluminium are 1.2 and 1.5 eV respectively). The creep of TD-Ni (Ni + 2 vol % $ThO_2$) also can be satisfactorily explained, below 0.5 $T_m$, by cross-slip [22], and the high-temperature creep of several recrystallised Ni-$ThO_2$ alloys (1 to 3 vol % $ThO_2$) by climb [23]. The creep

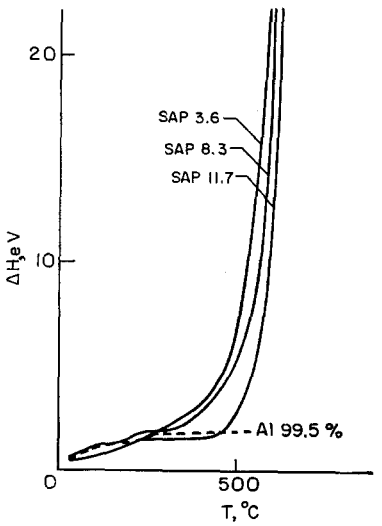


*Figure 6* Activation energy at constant strain rate as a function of temperature for SAP 3.6, 8.3, 11.7, and Al 99.5% ($\dot{\epsilon} = 2.7 \times 10^{-4}$ sec$^{-1}$, $\epsilon = 2 \times 10^{-3}$).

of Al-$Al_2Cu$ at high temperatures also has an activation energy close to the self-diffusion energy in pure aluminium [24]. The general equation for the strain rate resulting from the climb of edge dislocations by diffusion of jogs has to be applied [2]:

$$\dot{\epsilon} = \text{const.} \frac{1}{h} \exp\left(-\frac{U_D}{kT}\right) \sinh\left(\frac{nb^3\tau}{kT}\right)$$

where $U_D$ is the self-diffusion energy, $\tau$ the applied stress, $n$ a stress-concentration factor, and $h$ the mean height that a dislocation has to climb before escaping by glide or annihilation. If the escape takes place at the head of a piled-up group on a second-phase particle, $h$ has to be of the order of the half-height of the particle [25]; for a pile-up on inter-crystalline barriers, $h$ has to vary as $\tau^{-2}$.

Measurements of the activation volume made by Guyot on SAP [21] are in reasonable agreement with the values expected from the previous equation. (Note in this regard that the activation volume is equivalent to $kT\,(\mathrm{d}\ln\dot{\epsilon}/\mathrm{d}\tau)_T$.) Cross-slip and climb can be operative at lower temperatures (section 3.1.2) for higher strains and therefore higher stress levels.

#### *3.2.2. Other Processes*

The high activation energies measured above 350° C show that the high-temperature deformation mechanisms in SAP are radically different

from those in aluminium, since in the latter the climb of dislocations is the controlling process up to the melting point, with a constant activation energy close to the self-diffusion energy [26]. The variation of the activation energy with the temperature is apparent, because the tensile tests were conducted under low stress at high temperature, and vice versa. So the activation energy increases steeply with decreasing stress, as reported in references 12 and 21. Similar activation energies have been observed by other investigators in SAP [25, 27]. In fact, high values of activation energy, reaching 10 or more times the self-diffusion energy at high temperatures, seem to be a general feature for dispersion-hardened alloys: indium-glass composites [28], TD-Ni [23], and Ni-$Al_2O_3$ alloys [29]. Nevertheless, there is no general agreement concerning the stress dependence of the activation energy. Different models have been suggested depending on whether or not the apparent activation energy is a function of the stress.

(*a*) *Grain boundary sliding* Wilcox and Clauer [23] explained qualitatively, in terms of grain-boundary sliding, the stress-dependent activation energy for creep in TD-Ni. The presence of impurities or particles in the boundaries would increase the activation energy for sliding to the observed value. Nevertheless, the large stress exponent ($n = 40$) in the pre-exponential term of the strain rate remains difficult to explain.

(*b*) *Dislocation generation from grain boundaries* Ansell and Weertman [25] developed a semi-quantitative theory based on the generation of dislocations from grain boundaries. The activation energy of such a process is obviously strongly stress-dependent, but the expected grain-size dependence of the flow stress is not observed experimentally [12, 16].

(*c*) *Particles by-passed by glide* The model, based on the Orowan mechanism, consists of dislocations by-passing the particles intersecting the slip plane by thermally activated glide, for stresses lower than $\tau_c$. Calculations have been made by Coulomb [3] for particles softer than the matrix (or bubbles), and by Guyot [21] for particles harder than the matrix. In the last case, for small particles and for an applied stress very near the critical Orowan stress $\tau_c$, the activation energy is strongly stress-dependent:

$$\Delta H \simeq 2td\,[1 - (\tau/\tau_c)]^{3/2}$$

The numerical values agree well enough with the experimental ones for SAP, but the calculated activation volumes are between 10 and 100 times greater than the experimental ones [12].

(*d*) *Thermal activation of junction reactions* In alloys deformed at high temperatures, the particle-controlled recovery can still lead to large dislocation densities. Hirsch-type junction reactions [30] between attractive dislocations are frequently observed in this case [11]. Guyot has studied the thermal dissolution of such reactions [31]. The calculated activation energy and volume, which again vary rapidly with the applied stress, agree reasonably well with experimental data of SAP.

Even if the various models presented here are partially satisfactory, it is doubtful that a single model can, at high temperatures, uniquely describe the flow mechanism of this type of alloy. In any case, the large values of activation energy indicate a highly restricted dislocation mobility. Such alloys will therefore retain an appreciable flow stress, even at high temperatures.

## 4. The Nature of the Particle/Matrix Interface in Al-$Al_2O_3$ Alloys

As mentioned in the introduction, the knowledge of the nature of the particle/matrix interface is important for the study of the deformation mechanisms in metals containing a dispersed second phase, since the state of coherency of the interface controls the shearing of the particles by dislocations.

The nature of the particle/matrix interface can be studied by transmission electron microscopy, on the basis of contrast effects associated with either the particles or the matrix surrounding the particles. In the first case, the contrast effects can be due to different structure factors of particles and matrix or, alternatively, to the lack of a structural relationship of the particles with respect to the matrix. In the second case, the contrast effects are due to a strain field surrounding the particles. The strain field arises either from coherency or from differential thermal-contraction effects between particles and matrix, during cooling following an annealing treatment. The occurrence of the different types of contrast can be examined by changing the orientation of the specimen with respect to the electron beam.

Now we describe contrast studies by electron microscopy on Al-$Al_2O_3$ alloys of lower

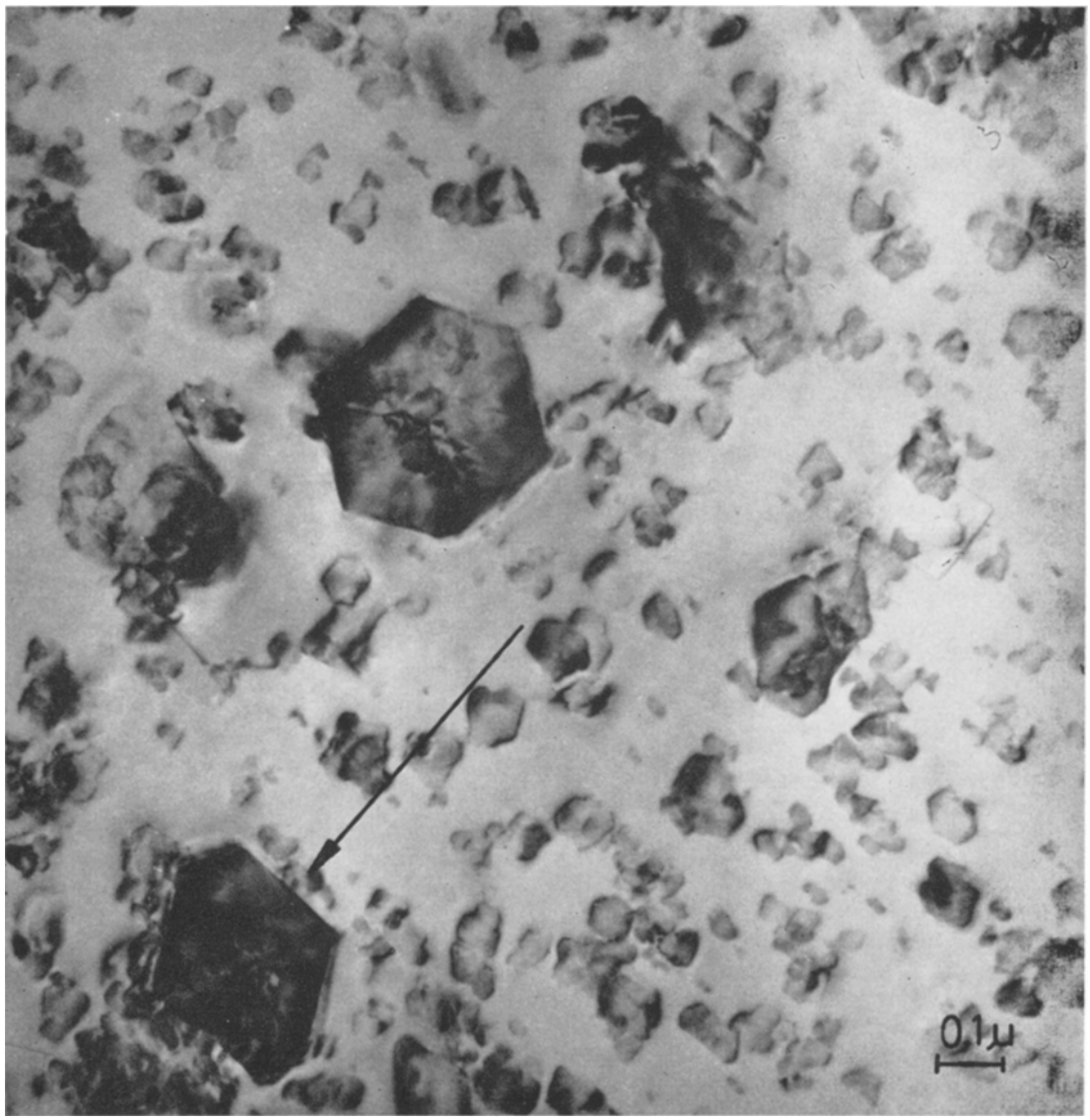


*Figure 7* Bright-field micrograph of SAP 4 foil prepared by cold-rolling and annealing at 630° C for 1 h. The alumina particles are imaged owing to the different structure factor of the alumina as compared with the matrix. Note the large particle, marked by an arrow, which is strongly diffracting owing to the lack of a simple structural relationship with the matrix.

alumina content ($\leqslant 4\%$). Fig. 7 is a bright-field micrograph of a SAP 4 foil showing the microstructure resulting from cold-rolling and recrystallisation at 630° C. The foil was oriented in such a way with respect to the electron beam that the alumina particles are imaged by structure-factor contrast, which reveals the true particle shape but not the surrounding strain field. As seen in fig. 7, the contrast of the larger alumina particles is not the same. For instance, the large particle marked by an arrow appears black, while other, larger particles appear lighter. By varying the foil orientation, it was observed that the contrast of the larger particles changed from dark to light or vice versa. Therefore, under particular tilting angles, the larger particles diffract strongly, whereas the surrounding matrix diffracts only weakly. This is a

strong indication that no simple structural relationship between the larger particles and the matrix exists.

The absence of a structural relationship is seen even more strikingly if one takes a selected-area diffraction pattern of regions including a larger particle. An example consisting of a complex spot pattern is shown in fig. 8. The less

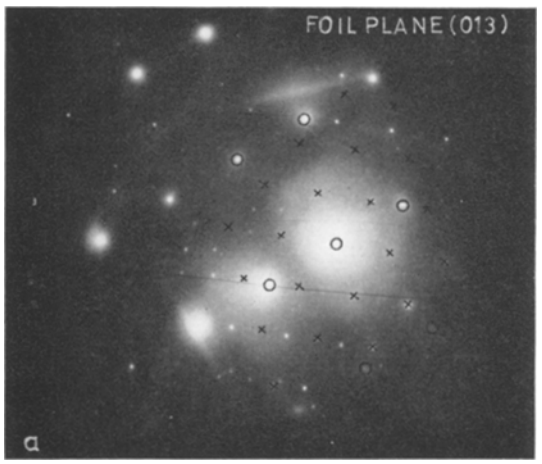


*Figure 8* Complex electron-diffraction pattern demonstrating the lack of a simple structural relationship between a large alumina particle and the matrix in the foil of fig. 7. The crosses represent the alumina spots for a (111) flat face. The circles correspond to the (013) aluminium-matrix plane.

intense spots marked by crosses are related to the reciprocal lattice of a large alumina particle. The spots marked by circles, on the other hand, belong to the reciprocal lattice of the aluminium matrix. One recognises that the alumina particle has the flat face in [1 1 1] orientation, and the foil plane of the aluminium matrix is approximately in [0 1 3] orientation. No prominent zone is parallel in the two lattices.

From the diffraction experiments, we can conclude that: (i) the flat face of the larger particles is (1 1 1) or (1 0 0); (ii) the flat face of the larger particles is randomly rotated in the foil plane; (iii) only very occasionally, a simple structural relationship of larger particles with respect to the matrix is observed.

By tilting the foil, the particles can also be imaged by another type of contrast, which arises from a strain field surrounding the particles. This type of contrast is shown in fig. 9. For particles located more to the centre of the foil, the contrast consists of a symmetrical pair of

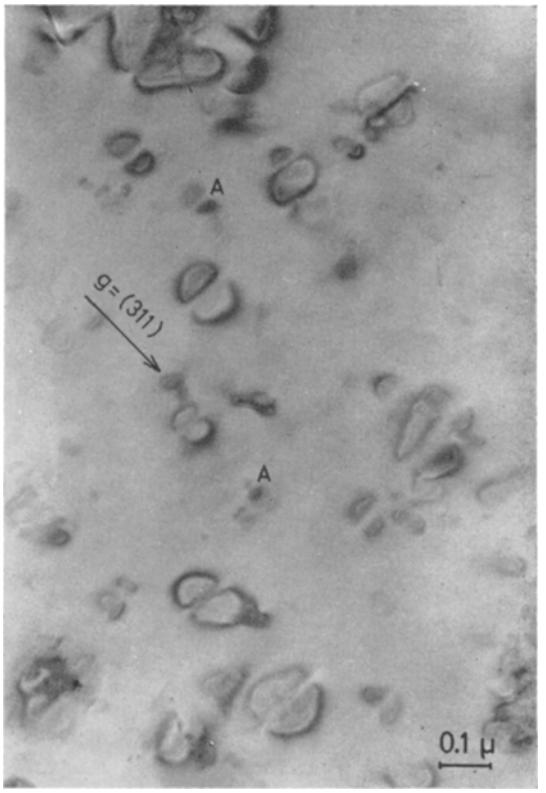


*Figure 9* Bright-field micrograph of the foil of fig. 7. The alumina particles are imaged owing to the presence of a strain field around the particles. Note the symmetrical images, as expected for a strain field around particles, at the centre of the foil. The asymmetrical images marked by A, on the other hand, are due to a strain field around particles close to the foil surface.

D-shaped lobes of equal intensity. The lobes are separated by a line of no contrast, which is perpendicular to the diffraction vector $\mathbf{g} = (3\,1\,1)$, giving contrast. For particles located close to each surface of the foil, on the other hand, one of the lobes is less intense and the whole image becomes asymmetrical, as shown for the particles marked by A.

Ashby and Brown have studied the contrast effects due to a symmetrical, spherical, strain field surrounding a particle, by dynamical theory, and have shown how the quantity and the sign of the strain parameter $\epsilon$ can be measured by electron microscopy [32, 33]. Results of a measurement of the quantity $\epsilon$ were given for a SAP 4 alloy in reference 34. Here we consider the determination of the sign of $\epsilon$, since it gives a conclusive answer about the origin of the strain around the particles in Al-$Al_2O_3$ alloys. Owing

to the smaller expansion coefficient of the alumina, the strain field arising from differential thermal-contraction effects between the particles and the matrix during cooling should be of positive sign, hence of "interstitial" type. Simple structural relationships between the particles and the matrix, which may lead to coherency, on the other hand, should give a strain field of negative sign, hence of "vacancy" type.

For determination of the sign of $\epsilon$, one uses the asymmetrical image of particles close to the foil surfaces [32, 33]. In bright field, for a strain field of uniform sign, the sense of asymmetry depends on whether the particles lie close to the bottom or to the top of the foil. In dark field, on the other hand, the sense of asymmetry remains the same, no matter to what surface the particles lie close. The sign can then be determined from the relationship between the sense of asymmetry and the positive direction of the diffraction vector. For instance, if the less intense lobe shows in the positive direction of the diffraction vector, then the strain field has a positive sign.

Fig. 10 represents a dark-field micrograph of the alloy of fig. 7. It is seen that the lobes with less intensity do show in the positive direction of the diffraction vector. Therefore, the strain field has a positive sign and is due to differential thermal-contraction effects and not to coherency.

In the original, extruded, Al-$Al_2O_3$ alloys, as used for the mechanical studies, the distribution of the particles is even more at random than in the rolled foils. Therefore, the absence of coherency in the rolled foils can be taken, with confidence, to imply also absence in the extruded alloys.


*Figure 10* Dark-field micrograph of the foil of fig. 7. Asymmetrical images, as expected for a strain field around particles close to the foil surface, are marked by arrows. Note that the less intense lobes show in the positive direction of the diffraction vector (**g** = 220), corresponding to a strain field of positive sign.

## Appendix

### Measurement of Dislocation Densities in Al-$Al_2O_3$ Alloys by Electron Microscopy

As shown in section 3.1.3, it is of particular interest to measure, in dispersion-hardened Al-$Al_2O_3$ alloys, the dislocation density by electron microscopy and to compare the directly measured values with those calculated from mechanical data.

We have tested the different electron-microscopy methods described in the literature for metals (see for instance reference 35), in order to find a suitable method for dispersion-hardened Al-$Al_2O_3$ alloys. The methods generally involve counting the intersection of dislocations with a unit area or a unit line length. We made use of the method described by Ham and Sharpe [36], which involves counts of the intersections between dislocations and the foil surface. This method, actually an extension of the etch-pit method, is not affected by any rearrangement of dislocations during thin-foil preparation, and the foil thickness is not needed. Furthermore, we made use of the methods described by Keh [37] and Ham [38], which consist of counting the intersections between dislocations and either a cross-grid of drawn lines or else randomly drawn lines. In fig. 11, which represents a deformed SAP 2.5 alloy, the systems of drawn lines as used by us for intersection counts are illustrated schematically. Furthermore, some end-points of dislocations at the surface as used by us for surface intersection counts are marked by crosses. It is

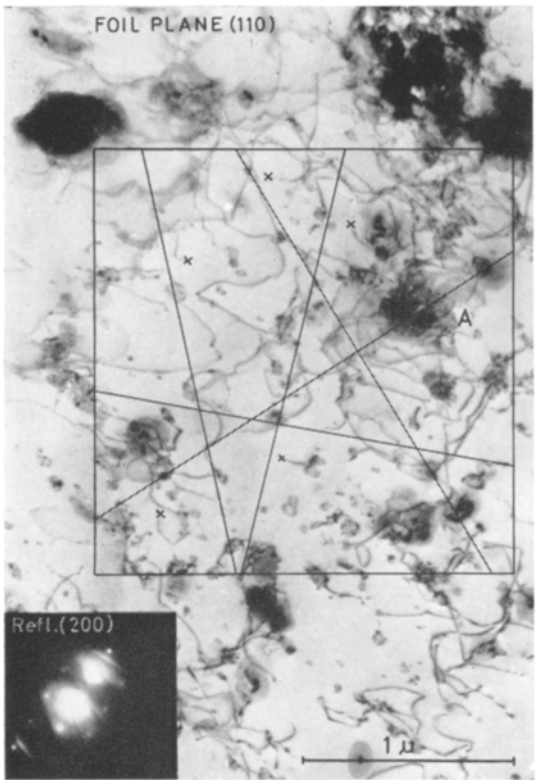


*Figure 11* Bright-field micrograph of SAP 2.5 foil prepared by cold-rolling and annealing at 630° C for 1 h after 4% tensile deformation. The foil plane is (110). The dislocations are imaged with the (200) reflection. The systems of drawn lines intersecting the dislocations, used for dislocation-density measurement, are schematically illustrated. Note the orthogonally drawn lines and the randomly drawn lines. The crosses mark dislocations ending at the surface, as used for surface intersection counts.

seen from fig. 11 that the dislocations are mainly concentrated around the large particle marked by A. It is also seen that the images of dislocations tangling around the large particle overlap. Hence their intersections with a drawn line are difficult to count. Also a correction has to be made for invisible dislocations. For fig. 11, a (200) reflection was used, therefore one-third of the dislocations are out of contrast. For the two methods of counting intersections between dislocations and drawn lines [37, 38], the thickness of the foil has to be known; it was deduced from slip traces, which, however, were not easy to obtain. We had to wait up to 15 min before dislocations started to move and slip traces appeared. This indicates that the dislocations are strongly pinned by the particles. Therefore, not too many dislocations should be lost during preparation of thin specimens.

In table III, the dislocation densities as obtained by different electron-microscopy methods for Al 99.9% and for SAP 2.5, deformed at room temperature, are compared. For the aluminium, the dislocation density values are roughly the same. For the SAP 2.5, on the other hand, the values obtained by the surface intersection method are lower by a factor of 2 to 3, as compared with the values obtained by the other two methods. Presumably the reason for this difference is a considerable fraction of dislocations, in deformed SAP, in the form of loops around or near the particles. The loops do not intersect the surface and are lost for surface intersection counts.

Concluding, we can say that suitable methods of measuring dislocation densities in dispersion-hardened alloys appear to be the methods involving intersection counts with a cross-grid of drawn lines or with a system of randomly drawn lines. We suggest that, in the case of Al-$Al_2O_3$ alloys, the correction factor accounting for the loss of dislocations during thin-foil preparation, at least at low deformations, is close to unity, or even is unity.

TABLE III Mean dislocation densities of Al 99.9% and SAP 2.5 deformed at room temperature, as obtained by electron microscopy. Values obtained by different methods of dislocation intersection counts.

| Specimen | Strain (%) | Mean density by surface intersection counts ($cm^{-2}$) [36] | Mean density by cross-grid intersection counts ($cm^{-2}$) [37] | Mean density by random-line intersection counts ($cm^{-2}$) [38] |
|---|---|---|---|---|
| Al 99.9% extruded | 0.2 | $(4.4 \pm 2.0) \times 10^9$ | $(4.0 \pm 2.0) \times 10^9$ | $(4.1 \pm 2.0) \times 10^9$ |
| SAP 2.5 recrystallised | 1.2 | $(1.5 \pm 1.5) \times 10^9$ | $(7.0 \pm 2.0) \times 10^9$ | $(7.2 \pm 2.0) \times 10^9$ |
| SAP 2.5 recrystallised | 1.5 | $(2.5 \pm 1.5) \times 10^9$ | $(7.5 \pm 2.0) \times 10^9$ | $(7.9 \pm 2.0) \times 10^9$ |

## References


1. E. OROWAN, Symposium on Internal Stresses, Inst. Met. (1947), p. 451.
2. J. FRIEDEL, "Dislocations" (Pergamon Press, 1964).
3. P. COULOMB, *Acta Met.* **7** (1959) 556.
4. E. GREGORY and N. J. GRANT, *Trans. AIME* **200** (1954) 247.
5. M. F. ASHBY and G. C. SMITH, *Phil. Mag.* **5** (1960) 298.
6. D. DEW-HUGHES and W. D. ROBERTSON, *Acta Met.* **8** (1960) 147.
7. M. F. ASHBY, "Electron Microscopy and Strength of Crystals" (Interscience, New York, 1963), p. 891.
8. P. B. HIRSCH, appendix to *J. Inst. Met.* **86** (1957) 7.
9. G. S. ANSELL, Bolton Landing Conference, Lake George, New York (1966), to be published.
10. A. KELLY and R. B. NICHOLSON, *Prog. in Matls. Sci.* **10** (1963) 10.
11. E. RUEDL and P. GUYOT, "Modern Developments in Powder Metallurgy", vol. 2 (Plenum Press, New York, 1966), p. 131.
12. P. GUYOT, Thèse de Doctorat, Paris (1965).
13. P. GUYOT and R. DEBEIR, *Acta Met.* **14** (1966) 43.
14. J. B. MITCHELL, S. K. MITRA, and J. E. DORN, *Trans. Quart. ASM* **56** (1963) 236.
15. G. SAADA, *Métaux et Corrosion* (July-September, 1960).
16. M. VON HEIMENDAHL and G. THOMAS, *Trans. AIME* **230** (1964) 1520.
17. M. F. ASHBY, *Z. Metalk.* **55** (1964) 5.
18. G. THOMAS, V. F. ZACKAY, and E. R. PARKER, "1965 Proceedings of the Sagamore Conference on High Strength Materials" (Syracuse University Press, in press).
19. H. G. SELL, W. R. MORCOM, G. W. KING, and N. F. CERULLI, Westinghouse Electric Corp, NY, Report TR 65-407 (1965).
20. J. C. FISHER, E. W. HART, and R. H. PRY, *Acta Met.* **1** (1953) 336.
21. P. GUYOT, *ibid* **12** (1964) 941.
22. B. A. WILCOX and A. H. CLAUER, *Trans. AIME* **236** (1966) 570.
23. *Idem*, op. cit. ref. 9.
24. W. H. GIEDT, O. D. SHERBY, and J. E. DORN, University of California, Inst. Eng. Research Report NR-031-048 No. 22 (1952).
25. G. S. ANSELL and J. WEERTMAN, *Trans. AIME* **215** (1959) 838.
26. O. D. SHERBY, J. LYTTON, and J. E. DORN, *Acta Met.* **5** (1957) 219.
27. C. L. MEYERS and O. D. SHERBY, *J. Inst. Met.* **90** (1961) 380.
28. T. D. GULDEN and J. C. SHYNE, *Trans. AIME* **227** (1963) 1088.
29. S. TAKAHASHI, K. IIDA, and M. ADACHI, *Trans. Jap. Res. Inst. for Metals* **6** (1965) 37.
30. P. B. HIRSCH, "Internal Stresses and Fatigue in Metals" (Elsevier, Amsterdam, 1959).
31. P. GUYOT, *Acta Met.* **14** (1966) 955.
32. M. F. ASHBY and L. M. BROWN, *Phil. Mag.* **8** (1963) 1083.
33. *Idem, ibid*, p. 1649.
34. E. RUEDL and E. STAROSTE, *J. Nucl. Matls.* **16** (1965) 103.
35. P. B. HIRSCH, "Electron Microscopy of Thin Crystals" (Butterworths, 1965), p. 422.
36. R. K. HAM and N. G. SHARPE, *Phil. Mag.* **6** (1961) 1193.
37. A. S. KEH, "Direct Observation of Imperfections in Crystals" (Interscience, New York, 1962), p. 213.
38. R. K. HAM, *Phil. Mag.* **6** (1961) 1183.